Available online at www.sciencedirect.com

ScienceDirect

Procedia CIRP 31 (2015) 471 – 476

www.elsevier.com/locate/procedia

15th CIRP Conference on Modelling of Machining Operations

A novel finite element approach to modeling hard turning in due consideration of the viscoplastic asymmetry effect

Eckart Uhlmann[a,*], Rolf Mahnken[b], Ivan Mitkov Ivanov[a], Chun Cheng[b]

[a]*Berlin Institute of Technology, Institute for Machine Tools and Factory Management, Pascalstraße 8–9, D-10587 Berlin, Germany*
[b]*University of Paderborn, Chair of Technical Mechanics, Warburger Str. 100, D-33098 Paderborn, Germany*

* Corresponding author. Tel.: +49-(0)30-314-23349; fax: +49-(0)30-314-25895. *E-mail address: eckart.uhlmann@ipk.fraunhofer.de*

Abstract

A novel material model for strain rate and temperature dependent asymmetric viscoplastic deformation behavior considering transformation induced plasticity (TRIP) as a crucial phenomenon influencing the hard turning process-oriented ductility was developed. Within the framework of viscoplasticity and continuum damage mechanics, the well-established Johnson-Cook flow stress model has been upgraded by the concept of weighting functions accounting for the asymmetric viscoplastic material behavior under different stress conditions during hard machining of chrome bearing steel AISI 52100. Moreover, the extended Johnson-Cook model incorporates the ductility alteration caused by transformation induced plasticity by applying the Leblond-approach. Based on the theoretical proceeding, a material routine for flow stress computation considering the viscoplastic asymmetry has been developed and applied within hard turning simulations using the commercial Finite-Element-Method (FEM) software DEFORM. In addition, the hard turning simulation model accounts for the phase transitions between martensite and austenite during the process-related material heating as well as austenite and white layer as a consequence of the so-called reverse martensite transformation. A decisive actuating variable concerning the feasibility and accuracy of the performed hard turning modelling is the austenite start temperature, which has been determined in consideration of the externally applied stress. Within the scope of the material modelling, a novel quantity referred to as stress mode factor has been introduced in order to enable the identification of areas in the cutting zone subjected to heterogeneous load conditions. The stress mode factor appraisal within the aforementioned bearing steel material routine discloses a new path to establish the influence of dissimilar stress states on the work piece heat balance as well as the impact of transformation induced plasticity on the stress distribution in the cutting zone.

Peer-review under responsibility of the International Scientific Committee of the "15th Conference on Modelling of Machining Operations
Keywords: Hard machining; Turning; Finite element method (FEM); Simulation; Material; Modelling

1. Introduction

Hard turning strives for substituting grinding as high-precision finishing manufacturing process of machined parts that exhibit hardness higher than 45 HRC [1]. The principal advantages of hard turning versus grinding are productivity increase, higher flexibility during chipping of geometrically intricate work pieces as well as resource efficiency [2,3,4]. The present research aims at investigating the potentiality of in-depth material modelling techniques in order to provide a basis for realistic hard turning simulation laying the groundwork for computer-aided process optimization. Furthermore, the inquest of the influence of the machine control variables relevant for the chip removal process during hard turning on the thermal and mechanical load collective allows for a better comprehension of surface zone damage causes as well as thermally induced manufacturing inaccuracies. With regard to the derivation of suitable measures for thermal and mechanical work piece stress diminution, an extensive hard turning simulation model accounting for phase transformations induced by temperature gradients at high strain rate plastic deformations as well as white layer formation ought to be developed and calibrated.

By means of experimental evaluation of the resultant force components during hard turning as well as the cutting edge microgeometry characteristics, a widespread set of measurement data was acquired with the objective of simulation model validation. Moreover, the work piece

Peer-review under responsibility of the International Scientific Committee of the "15th Conference on Modelling of Machining Operations
doi:10.1016/j.procir.2015.03.093

surface temperature that occurs under variable cutting conditions was identified applying a particular method using correction factors in order to estimate accurate temperature values based on a thermographic survey at a constant emissivity. The concomitant hard turning modelling was performed using the Finite-Element-Method (FEM) as a predominant approach for thermal and mechanical load collective evaluation of machining processes [5]. In this context, a novel material model for chrome bearing steel AISI 52100 considering the strain, strain rate and temperature dependent asymmetric viscoplastic yield stress behavior as well as the transformation induced plasticity (TRIP) as an essential phenomenon that affects the process-oriented ductility was developed. Within the scope of viscoplasticity and continuum damage mechanics, the well-known Johnson-Cook flow stress model has been extended by the concept of weighting functions incorporating the asymmetric viscoplastic material behavior under different load conditions during hard turning of chrome bearing steel AISI 52100 [6]. Based on the theoretical foundations, a material routine for flow stress computation accounting for the viscoplastic asymmetry has been implemented and integrated within hard turning simulations in the commercial FEM-software DEFORM. Furthermore, the performed simulation modelling describes the phase transitions between martensite and austenite during the process-dependent substance heating as well as austenite and white etching layer as a consequence of the reverse martensite transformation.

A crucial determining factor related to the feasibility and exactitude of the accomplished hard turning modelling is the austenite start temperature, which has been ascertained having regard to the externally applied stress impact. To achieve this objective, a simulation method has been applied and verified through an analytical approach. Within the framework of the performed material modelling, a novel quantity designated as stress mode factor has been derived in order to facilitate the identification of cutting zone areas subjected to heterogeneous load conditions. The stress mode factor assessment within the above-named bearing steel material routine initiates a new way to analyse the impact of diverse stress states on the work piece heat balance. Moreover, subsequent to a performed implementation of complementary physical phenomena within the material routine, such as the transformation induced plasticity, the respective influence on the stress distribution in the cutting zone can be examined.

2. Experimental procedure

In order to evaluate and calibrate the performed hard turning modelling, cutting trials of bearing rings IR 70X80X30 consisting of chrome bearing steel AISI 52100 with a surface hardness of 62 HRC were conducted. In this context, the *cutting speed* v_c, the *feed rate* f as well as the *depth of cut* a_p represent appropriate machining parameters to be variegated for the purpose of validating a turning process simulation model [7]. The used cutting tools exhibit the specification CNMA 120408 and are composed of carbide metal base plates as well as soldered polycrystalline cubic boron nitride inserts. Since the cutting insert microgeometry exerts a crucial influence on the thermal and mechanical work piece load collective, its characteristic traits were experimentally determined. In this manner, the *width of the cutting edge chamfer* and the *angle of chamfer* were established to equal $b_f = 0.15$ mm and $\gamma_f = 53°$ respectively. Moreover, considering the tool holder *clearance angle* of $\alpha = 6°$, the *effective rake angle* equals $\gamma_{eff} = -59°$. In addition, the cutting edge exhibits a *radius between rake face and chamfer* of $r_\gamma = 39$ µm as well as a *radius between flank face and chamfer* of $r_\alpha = 41$ µm.

The cutting trials were conducted at a Computerized Numerical Control (CNC) turning and milling center TRAUB TNX 65. The work piece outer surface was turned and the resultant force components were ascertained using a Kistler dynamometer of type 9121. In this regard, the *cutting speed* was varied between $v_{c1} = 100$ m/min and $v_{c2} = 200$ m/min. The measurement results confirm that the resultant force components do not depend on the *cutting speed* v_c, due to the neutralization of higher material removal rates and higher cutting forces at increasing *cutting speed* v_c, temperature rise, substance softening and concomitant diminishment of the rake face friction coefficient [8]. In conclusion, the accomplished hard turning modelling is evaluated by means of the acquired measurement data and the resulting flow chip formation.

Due to the multitudinous influencing variables affecting the accurateness of the performed contactless radiation temperature measurement approach, a thermographic camera of type JADE II MWIR manufactured by InfraTec GmbH, Dresden, Germany, was gauged using a particular methodology. For this purpose, an *initial representative temperature value* of $T_i = 700°C$ was determined. The aforesaid temperature level depends on the manufacturing process to be analyzed, the material to be machined, its hardness and surface integrity, stating that the expected temperature values exhibit only a slight deviation from the initially defined fundamental temperature magnitude T_i. Subsequently, specimens were heated to T_i utilizing a test rig especially created for precise temperature setting. Using the evaluation software of the aforementioned thermographic camera, the specimen surface emissivity was continuously varied until the measured surface temperature value equals T_i. Thus, the work piece surficial *emissivity* ε_i valid for the *representative temperature level* T_i was established. Afterwards, the specimen surface temperature was variegated around T_i at the experimental rig and gauged at a constant *emissivity* of ε_i. Since the test piece emissivity depends on the corresponding surface temperature, the executed measurements at a constant *emissivity* ε_i delivered incorrect results. Nevertheless, a correction factor trend as a function of the illegitimately ascertained specimen surface temperature at a constant emissivity was derived. Thus, the multiplication between an arbitrary incorrect temperature value around T_i and the appendant correction factor yields the real specimen surface temperature.

During the conducted specimen surface temperature measurements in a representative range of $T_i = 700 \pm 200°C$, the emissivity value adjusted in the evaluation software of the applied thermographic camera equals ε_i. For this purpose, bearing rings IR 70X80X30 were clamped and thereafter machined at a CNC turning and milling center TRAUB TNX 65. The temperature values of single points on the specimen

surface straight before the onset of chip formation were detected through the aforementioned analysis software of the thermographic camera used to record the hard turning process. Subsequently, the temperature data measured at an *emissivity* of ε_i were multiplied by the corresponding correction factor for the purpose of calculating the accurate process-dependent work piece surface temperature.

The described temperature evaluation method was adapted for application to both oxidized and not oxidized surfaces adjusting the respective correction factor gradient. In order to suppress the specimen surface oxidation, a purpose-built facility which purges the measurement plane by use of carbon dioxide was applied. It should be emphasized that, even if the depicted temperature computation procedure yields satisfactory results, the uncertainness regarding a potential intermediate specimen surface state between entirely oxidized and not oxidized during the hard turning process exhibits a supposable error source. Nonetheless, it is advisable to apply the correction factor gradient obtained in the case of not oxidized specimen surfaces during machining experiments, since the extremely rapid heating-up and cooling rates that distinguish the hard turning process prevent any remarkable superficial oxidation.

Fig. 1 illustrates the specimen surface temperature values determined on single checkpoints straight before the initiation of chip formation applying the described correction factor procedure. During the machining experiments, the *cutting speed* v_c, the *depth of cut* a_p, the *feed rate* f and the *tool cutting edge angle* κ were varied. The obtained measurement data did not reveal any dependence of the estimated temperature values on the *tool cutting edge angle* κ at a *cutting speed* of $v_c = 100$ m/min. In contrast, a slight temperature decrease with a rising *tool cutting edge angle* κ could be ascertained at a *cutting speed* of $v_c = 200$ m/min, which can be explained by the impact of the cutting velocity and the coherent material removal rate on the friction conditions in the cutting zone, the temperature height, the resultant force components, the chip shape and the contact area between work piece and tool. When increasing the *cutting speed* from $v_c = 100$ m/min to $v_c = 200$ m/min, a temperature rise on the machined specimen surface straight before the onset of chip formation at *tool cutting edge angles* of $\kappa = 90°$ and $\kappa = 95°$ could be established. A similar interdependence between the maximum temperature values in the cutting zone and the *cutting speed* v_c at a *tool cutting edge angle* of $\kappa = 99.9°$ was not given. In addition, no discernible dependency of the analyzed temperature level on the *tool cutting edge angle* κ at a constant *depth of cut* a_p as well as nonvarying *feed rate* f could be identified. Similarly, a feed rate variation at an unaltered *tool cutting edge angle* κ did not reveal any remarkable surface temperature dependence. In conclusion, it could be established that at a *tool cutting edge angle* of $\kappa = 90°$, the maximum temperature magnitude on the specimen surface prior to the chip formation decreases with higher *depths of cut* a_p, whereas a temperature rise at *tool cutting edge angles* of $\kappa = 95°$ and $\kappa = 99.9°$ was observed.

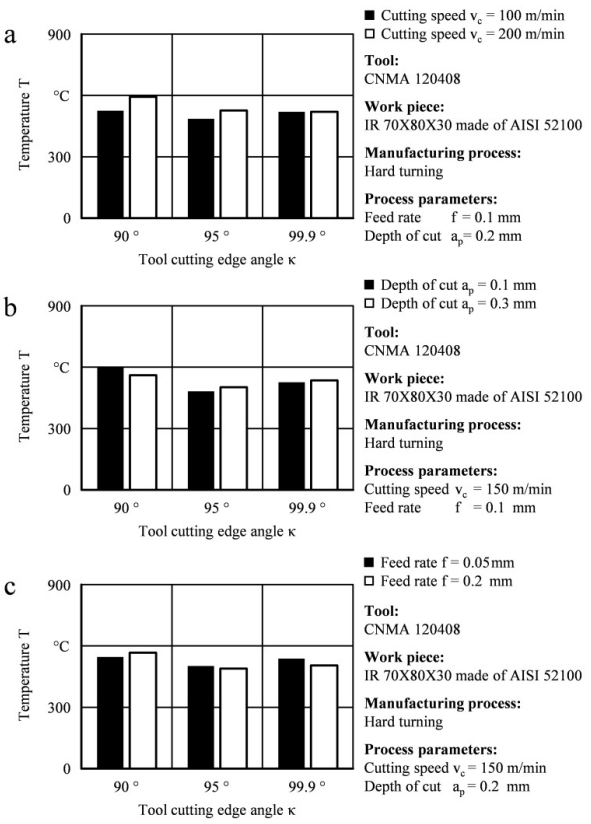

Fig. 1. Specimen surface temperature straight before the onset of chip formation computed applying the correction factor procedure
(a) variation of the cutting speed v_c;
(b) variation of the depth of cut a_p;
(c) variation of the feed rate f.

3. Extension of the Johnson-Cook flow stress model by the strength difference effect (SD-effect)

Machining experiments using high strength steel specimens substantiate a different yield stress behavior under dissimilar load conditions such as tension, compression and shear [9]. Hence, martensitic steel exhibits higher yield stresses in compression compared to tension [10]. This peculiar material characteristic is referred to as strength-difference effect (SD-effect) or asymmetric effect. Numerous publications place emphasis on an accurate modelling and simulation of the plastic material behavior considering the SD-effect. The majority of the approaches for a proper asymmetric effect description is based on a stress potential that depends on the stress tensor as well as further variables specifying the state of hardening, softening or damage [10].

An exemplary approach utilizes the so-called *stress mode angle* or *Lode angle* θ_m in order to reveal asymmetric effects [6]. Furthermore, the aforesaid quantity is also applied to introduce the concept of stress mode dependent weighting functions and thus model creep phenomena considering asymmetric effects. Therefore, the well-known Johnson-Cook model is intended to be modified and extended by the concept of weighting functions in order to account for asymmetric effects within a small strain framework. Up to the present, the

total *strain* ε experienced by a work piece volume element is being additively decomposed, Eq. (1):

$$\varepsilon = \varepsilon_e + \varepsilon_p \tag{1}$$

In this context, the elastic part ε_e is being related to the stress tensor $\boldsymbol{\sigma}$ by the Hooke's law. Moreover, the plastic part ε_p can be ascertained from evolution equations determining its time derivative $\dot{\varepsilon}_p$. The derivation of a flow stress material model in due consideration of the SD-effect commences by specifying a yield function based on the well-known Johnson-Cook formulation having regard to the temperature and strain rate dependence of the plastic material behavior. Furthermore, applying the concept of weighting functions, an enhancement of the Johnson-Cook flow stress model enabling it to describe the asymmetric plasticity of materials at high strain rates and temperature levels in machining simulations can be performed. The original formulation of the Johnson-Cook model is proposed for the *von Mises stress* σ_v, Eq. (2):

$$\sigma_v = \left(A + B \cdot e_v^n\right) \cdot \left(1 - T^{*m}\right) \cdot \left(1 + C \cdot \ln \frac{\dot{e}_v}{\dot{\varepsilon}_0}\right) \tag{2}$$

In Eq. (2), e_v signifies the *equivalent plastic strain*, T^* the *homologous temperature* value and A, B, C, n, m as well as $\dot{\varepsilon}_0$ material parameters. Furthermore, the factor A designates the *initial yield stress*, B and n describe the effect of strain hardening, C and $\dot{\varepsilon}_0$ illustrate the plastic strain rate dependency of the yield stress magnitude, whereas m depicts the effect of adiabatic heating. Based on the primal Johnson-Cook equation, a yield function is specified according to Eq. (3):

$$\Phi = \sigma_v - \left(Y_0 + Q_1 + Q_2\right) \cdot \left(1 - T^{*m}\right) \cdot \left(1 + C \cdot \ln \frac{\dot{e}_v}{\dot{\varepsilon}_0}\right) \tag{3}$$

Eq. (3) comprises the *von Mises stress* which is being expressed in terms of the deviatoric part of the stress tensor. Comparing Eq. (2) and Eq. (3), the hardening stress term $B \cdot e_v^n$ is substituted by the summation of the hardening stresses $Q_1[e_v] = Q_0 \cdot \left(1 - \exp\left(-b \cdot e_v\right)\right)$ and $Q_2[e_v] = H \cdot e_v$ for a non-linear and linear hardening, respectively. Moreover, the stress mode dependent weighting functions w_i are defined according to Eq. (4.1 and 4.2):

$$4.1 \quad \sum_{i=1}^{S=3} w_i[\boldsymbol{\sigma}] = 1 \qquad 4.2 \quad w_i\left[\boldsymbol{\sigma}_j\right] = \delta_{ij} \tag{4}$$

In this context, the weighting functions w_i are associated with independent representative stress modes, that are characterized by appendant stress tensors $\boldsymbol{\sigma}_j$, j = 1,2,…,S, [6]. Furthermore, Eq. (4.1) can be considered as a completeness condition, while Eq. (4.2) illustrates a normalization condition for the weighting functions. The mathematical formulation of the concept of stress mode dependent weighting functions is based on the quantities represented by Eq. (5) [6]:

$$5.1 \quad \xi = \frac{\sqrt{27}}{2} \cdot \frac{J_{3d}}{\left(J_{2d}\right)^{\frac{3}{2}}}, \; -1 \le \xi \le 1 \qquad 5.2 \quad \theta_m = \frac{1}{3} \cdot \arccos[\xi] \tag{5}$$

The quantity θ_m is referred to as the *stress mode angle* and is contingent upon the *stress mode factor* ξ. Moreover, J_{2d} and J_{3d} designate the second and third *stress invariant*, respectively. The three unequal stress modes are being associated with the three loading types of tension, compression and shear. Consequently, Eq. (4.1) and Eq. (4.2) are satisfied by means of weighting functions dependent on the *stress mode factor* ξ, Eq. (6) – Eq. (8):

$$w_1 = \begin{cases} \xi^2, if\ \xi \ge 0 \\ 0, else \end{cases} \tag{6}$$

$$w_2 = \begin{cases} \xi^2, if\ \xi \le 0 \\ 0, else \end{cases} \tag{7}$$

$$w_3[\xi] = 1 - \xi^2 \tag{8}$$

Here, the quantities w_1, w_2 and w_3 denominate the corresponding weighting functions for tension, compression and shear load, respectively. Furthermore, the evolution equation of the plastic strain tensor time derivative in Eq. (1) can be expressed through Eq. (9):

$$\dot{\boldsymbol{\varepsilon}}_{\boldsymbol{p}} = \dot{\lambda} \cdot \sqrt{\frac{3}{2}} \cdot \bar{\boldsymbol{N}} \tag{9}$$

The quantity $\bar{\mathbf{N}}$ denominates the flow direction and can be determined by the use of Eq. (10):

$$\bar{\boldsymbol{N}} = \frac{\boldsymbol{\sigma}^{\boldsymbol{dev}}}{\left\|\boldsymbol{\sigma}^{\boldsymbol{dev}}\right\|} \tag{10}$$

The *plastic multiplier* $\dot{\lambda}$ can be derived from the Kuhn-Tucker conditions, Eq. (11):

$$\dot{\lambda} \ge 0, \dot{\lambda} \cdot \Phi = 0, \Phi \le 0 \tag{11}$$

In this context, the rate of *equivalent plastic strain* $\dot{e}_v$ can be ascertained through Eq. (12):

$$\dot{e}_v = \sqrt{\frac{2}{3} \dot{\boldsymbol{\varepsilon}}_{\boldsymbol{p}} : \dot{\boldsymbol{\varepsilon}}_{\boldsymbol{p}}} = \dot{\lambda} \cdot \sqrt{\frac{2}{3} \frac{3}{2} \bar{\boldsymbol{N}} : \bar{\boldsymbol{N}}} = \dot{\lambda} \tag{12}$$

Table 1 comprises all required equations in order to characterize the hard turning simulation model considering the viscoplastic asymmetry effect. In this context, the yield function Φ represents a threshold term for the *von Mises stress* σ_v. Moreover, the quantity Y_0 illustrates an initial margin for plastic material behavior that is being augmented by the hardening stress terms Q_1 and Q_2. In addition, the SD-effect is incorporated within the framework of the described material modeling of chrome bearing steel AISI 52100 by means of constants computable on the basis of the above-named weighting functions. Due to the heavy dependence of the weighting functions on the stress invariants, the weighted constants as a substantial part of the yield function consider the current stress state in the machined work piece during the performed hard turning simulations.

Table 1. Summarization of a model for asymmetric visco-plasticity.

Flow rule	$\dot{\varepsilon}_p = \dot{\lambda} \cdot \sqrt{\frac{3}{2}} \cdot \bar{N}$
Flow direction	$\bar{N} = \frac{\sigma^{dev}}{\left\|\sigma^{dev}\right\|}$
Flow factor	$\dot{\lambda} = \dot{e}_v = \sqrt{\frac{2}{3}\dot{\varepsilon}_p : \dot{\varepsilon}_p}$
Yield function	$\Phi = \sigma_v - \left(Y_0 + Q_1 + Q_2\right) \cdot \left(1 - T^{*m}\right) \cdot \left(1 + C \cdot \ln \frac{\dot{e}_v}{\dot{\varepsilon}_0}\right)$
Hardening stresses	$Q_1[e_v] = Q_0 \cdot \left(1 - \exp\left(-b \cdot e_v\right)\right) \quad Q_2[e_v] = H \cdot e_v$
Weighted constants	$Y_0 = \sum_{i=1}^{S} w_i \cdot Y_{0i} \qquad Q_0 = \sum_{i=1}^{S} w_i \cdot Q_{0i}$
	$H = \sum_{i=1}^{S} w_i \cdot H_i \qquad b = \sum_{i=1}^{S} w_i \cdot b_i$
	$C = \sum_{i=1}^{S} w_i \cdot C_i \qquad m = \sum_{i=1}^{S} w_i \cdot m_i$
Material parameters	$\boldsymbol{\kappa_{pi}} = \left[Y_{0i}, Q_{0i}, H_i, b_i, C_i, \varepsilon_{0i}, m_i\right]^T \; i = 1,...,S$

4. Hard turning model extension by the transformation induced plasticity effect on the process-oriented material ductility

The transformation induced plasticity impact on the process-related material ductility as well as the specimen surface temperature level is being considered within the hard turning simulation model through the Leblond approach [11]. Fig. 2 illustrates the temperature profiles of exemplary checkpoints on the machined surface at a cutting distance of s = 1.9 mm relative to the machining starting point using the described flow stress governing equations. The lowest temperature values that have been ascertained on the specimen surface result from simulation calculations using wear-free cutting tool models, whereas the highest surface thermal load occurs in case of worn tools without consideration of the TRIP effect. Furthermore, the highest difference between the estimated temperature maxima in the work piece surface layer when comparing the simulation results with and without consideration of the TRIP effect could be determined at the interface between the flank wear land and the specimen surficial area. In addition, Fig. 2 depicts the thermal load decrease as a consequence of the implementation of the Leblond approach as well as the contiguous ductility increase of chrome bearing steel AISI 52100. The surface layer temperature gradients disclose the occurrence of two thermal peaks in case of worn tools, which can be attributed to the impingement between the cutting edge and the analyzed specimen face checkpoints as well as the subsequent friction between work piece and flank wear land. In opposition to the temperature and stress level alteration through the implementation of the Leblond approach, no significant variation of the stress mode factor distribution in the cutting zone could be established. Thus, the

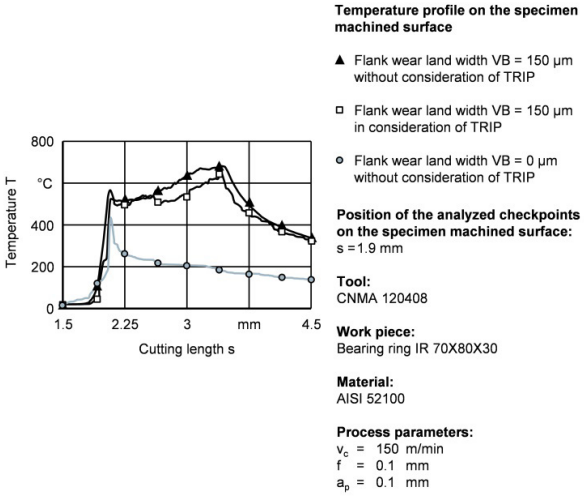

Fig. 2. Transformation induced plasticity influence on the temperature profile on the machined specimen surface

conclusion can be drawn that the transformation induced plasticity exerts no substantial influence on the stress distribution in the cutting area. Finally, it is denotative to emphasize the satisfactory agreement between the maximum temperature value calculated at a *width of flank wear land* VB = 0 µm (see Fig. 2) and the corresponding, experimentally determined temperature magnitude under equal cutting conditions (see Fig. 1).

5. Evaluation of the influence of the stress state in the cutting area on the austenitizing temperature

In order to model phase transitions of chrome bearing steel AISI 52100 during machining under the assumption of exclusively temperature-driven austenitization and white layer formation as a consequence of the reverse martensite transformation, the determination of the corresponding microstructure conversion temperature is required. Based on experimentally proved knowledge of machining conditions capable of arousing white layer appearance on the surface of hard turned bearing races, equivalent simulation calculations using the described material model were performed. It seems likely that an *austenitizing temperature* variation within the FE-model allowing for tool wear results in unequally wide white layers. The simulated and experimentally determined white layer thicknesses coincide for an *austenitizing temperature* of $T_A = 650$ °C. Furthermore, the pertinence of the numerically ascertained stress-induced *austenite transition temperature shift* ΔT_A could be approved using the Clausius-Clapeyron equation [9]. The solution of the aforesaid mathematic approach requires the knowledge of the phase transformation energy, the nominal transition temperature, the volume dilatation, which is calculable through the molar mass and phase densities, as well as the maximum pressure variation in the cutting area that has been evaluated by dint of simulation calculations [12]. Hence, the analytical approach yields a stress-induced *austenitizing temperature* of $T_{A,S} = 681.89$ °C, which differs from the FE-model-based value by less than 5 % and emphasizes the satisfactory

agreement between the thermodynamic fundamentals and the accomplished FE-modelling.

6. Influence of dissimilar stress states in the cutting zone on the work piece heat balance

On the basis of the theoretically developed approach to identify areas in the cutting zone subjected to dissimilar stress conditions by means of the *stress mode factor* ξ, the generated chrome bearing steel material routine is capable of establishing high compressive stress regions in the chip root as well as low tensile stress spots beneath the cutting edge affecting the reached temperature level and the machined surface quality. Consequently, an incentive to derive a procedure which evaluates the cutting zone stress distribution influence on the work piece heat balance is provided. By means of the algebraic sign of the *stress mode factor* ξ attributed to each specimen volume element using the commercial FEM-software DEFORM, the appendant stress state can be determined, the correspondent yield stress magnitude in the material routine deliberately decreased and the subsequent impact on the machined surface temperature level analyzed. Thus, Fig. 3 illustrates the average temperature profiles of an exemplary checkpoint on the work piece machined surface both in and without consideration of the compressive stress in the cutting zone. Hence, the tensile stress appearing underneath the cutting edge has no perceptible impact on the work piece heat balance. Moreover, disregarding compression stress in the work piece material routine yields a calculation error of approximately 80 %. In general, this procedure can be applied for the simulation of any chip-removing manufacturing process with the objective of gaining a better understanding of the stress distribution in the work piece cutting zone as well as analyzing the influence of dissimilar stress conditions on the temperature development in the surface layer.

7. Summary and outlook

The present study describes the experimental investigations of the resultant force components and the surface temperature during hard turning of bearing steel AISI 52100 with the aim of calibrating a FE simulation model. Moreover, the Johnson-Cook model has been upgraded by the concept of weighting functions in order to incorporate the asymmetric viscoplastic material behavior. A crucial phenomenon referred to as transformation induced plasticity has been considered by parameterizing the Leblond-approach. Furthermore, the dependence of the austenitizing temperature on the externally applied stress has been determined. According to the theoretical proceeding, a novel quantity referred to as stress mode factor and its applicability have been presented.

The illustrated findings encourage further numerical research using worn inserts with the purpose to analyze the stress mode factor distribution inside the cutting edge as well as a possible correlation between the flank wear land development and the stress mode factor apportionment. Moreover, a far-reaching comprehension of the work piece stress allocation using complex tools can be expected.

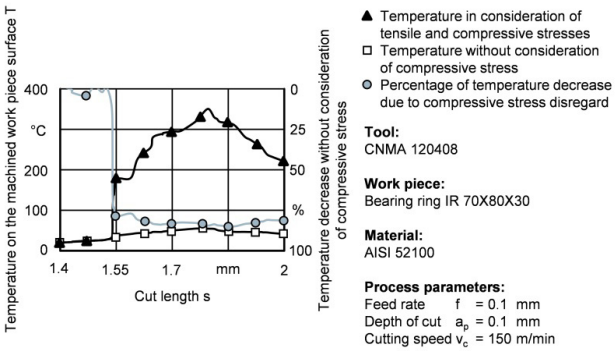

Fig. 3. Influence of the compressive stress in the cutting zone on the temperature development in the work piece surface layer

Acknowledgements

The authors thank the German Research Foundation for its financial support within the Priority Program 1480.

References

[1] Umbrello D, Ambrogio G, Filice L, Shivpuri R. An ANN approach for predicting subsurface residual stresses and the desired cutting conditions during hard turning. Journal of Materials Processing Technology 2007; 189, p. 143-152.
[2] Tönshoff HK, Arendt C, Ben Amor R. Cutting of hardened steel. CIRP Annals 2000; 49/2, p. 547-566.
[3] Byrne G, Dornfeld D, Denkena B. Advancing Cutting Technology. CIRP Annals 2003; 52/2, p. 483-507.
[4] Rech J, Moisan A. Surface integrity in finish hard turning of case hardened steels. International Journal of Machine Tools and Manufacture 2003; 43, p. 543-550.
[5] Uhlmann E, Graf von der Schulenburg M, Gerstenberger R. Investigations on the adjustment of the modelling section in 2D simulations of milling processes. International Journal of Machining and Machinability of Materials 2009; 6:1-2, p. 69-82.
[6] Mahnken R. Creep simulation of asymmetric effects at large strains by stress mode decomposition. Computer Methods in Applied Mechanics and Engineering 2005; 194:39-41, p. 4221-4243.
[7] Biermann D, Höhne F, Sieben B, Zabel A. Finite element modeling and three-dimensional simulation of the turning process incorporating the material hardness. International Journal of Material Forming 2010; 3-1, p. 459-462.
[8] Biermann D, Liedschulte M. Plasmaunterstütztes Drehen von Hartlegierungen auf Eisenbasis mit PKB. Industrie Diamanten Rundschau 1994; 28-2, p. 71-77.
[9] Uhlmann E, Mahnken R, Ivanov IM, Cheng C. FEM modeling of hard turning with consideration of viscoplastic asymmetry and phase transformation. Journal of Machine Engineering 2013; 13/1, p. 80-92.
[10] Spitzig WA, Sober RJ, Richamond O. Pressure dependence of yielding and associated volume expansion in tempered martensite. Acta Metallurgica 1975; 23, p. 885-893.
[11] Leblond JB. Mathematical modeling of transformation plasticity in steels II: coupling with strain hardening phenomena. Int. J. of Plasticity 1989; 5, p. 537-591.
[12] Ramesh A, Melkote SN. Modeling of white layer formation under thermally dominant conditions in orthogonal machining of hardened AISI 52100 steel. International Journal of Machine Tools & Manufacture 2008; 48, p. 402-414.